Manuscript for *Revista Mexicana de Astronomía y Astrofísica* (2007)

ABSOLUTE ELEMENTS FOR THE NEAR CONTACT ECLIPSING BINARY V878 HERCULIS

R. H. Nelson,[1,2,3] K. B. Alton,[2] M. R. Kendurkar,[3] K. Stępień[4]

Draft version: August 27, 2024

RESUMEN

ABSTRACT

New radial velocity (RV) and light curve (LC) data for the near contact eclipsing binary V878 Her have been simultaneously modeled with the Wilson-Devinney code (WD2003). Two distinct LC datasets were investigated: one was from the Transiting Exoplanet Survey Satellite (TESS) while the others were acquired from the ground-based Mountain Ash Observatory (MAO) in British Columbia, Canada. Supporting spectroscopic data were acquired using the 1.83-m Plaskett Telescope at the Dominion Astrophysical Observatory (DAO) between 2009-2020. Preliminary results from our RV investigations produced values for K_1 (-101.7 ± 4.3 km·s^{-1}), K_2 (219.5 ±.4 km·s^{-1}), V_γ (-34.4 ± 5 km·s^{-1}), and q_{sp} (0.464 ± 0.040). Potential progenitors of this near contact binary (NCB) were evaluated using an evolutionary model derived from cool close binaries. It is argued that V878 Her is not in the thermal relaxation oscillation (TRO) phase but, instead, it is a first timer, i.e. in a state of contact binary formation. Its most probable ZAMS progenitor had masses equal to about 1.7 and 0.6 $M_\odot$ and the orbital period of about 1.6 days.

Key Words: Stars: binaries: eclipsing — Stars: evolution — Stars: fundamental parameters — Stars: binaries: spectroscopic — Stars: imaging

1. INTRODUCTION

Near contact binaries (NCBs) have been identified as a separate class of binaries by Shaw (1990) who distinguished two types of NCBs: V1010 Oph type and FO Vir type. Yakut & Eggleton (2005) suggested the names SD1 and SD2 for NCBs of V1010 Oph and FO Vir type, respectively. SD1 binaries consist of primaries filling their critical Roche lobes and transfering matter through the Lagrangian point L1 to slightly oversized (by a factor of ~ 1.2) secondaries whereas SD2 binaries resemble short period Algol-type variables. We will use the designations SD1 and SD2 herein.

After finding evidence for variability from photographic plates, Kaiser (1994) confirmed that V878 Her (aka SAO 46698, BD-49 2630, TYC 3516-0047-1, and TIC 188766090) was variable using photoelectric detection. The

[1]Mountain Ash Observatory, 1393 Garvin Street, Prince George, BC, Canada, V2M 3Z1
[2]Desert Blooms Observatory, 70 Summit Ave., Cedar Knolls, NJ, 07927, USA
[3]Guest investigator, Dominion Astrophysical Observatory, 5071 W Saanich Rd, Victoria, BC V9E 2E7, Canada
[4]Warsaw University Observatory, Al. Ujazdowskie 4, 00-478 Warszawa, Poland

first linear ephemeris was reported in another study (Kaiser et al. 1996) which described this system as a "thermally decoupled binary of W UMa or near contact (NCB) type". Later on Bloomer & Ngwele (1999) produced new CCD-derived light curves in V- and R-passbands from which newly derived light elements showed no significant changes compared to those reported earlier by Kaiser et al. (1996). A spectroscopic study (Popper 1996) indicated that V878 Her was close to type F5. Cross correlation of positional data found in the SuperWASP and ROSAT archives indicated that the location of this variable star was coincident with an X-ray source (Norton 2007) thereby suggesting significant stellar coronal activity (Rosner et al. 1985; Hartman & Noyes 1987). Hoffman et al. (2008) classified V878 Her as a β Lyrae type candidate based on light curve data from the Northern Sky Variability Study (NSVS). Other than times-of-minima which have been sporadically published over the past 45 years, no definitive characterization of this eclipsing binary system has been found in the literature. Herein, new radial velocity data simultaneously modeled with multi-bandpass light curves has resulted in a far more robust physical, geometric and evolutionary characterization of V878 Her.

2. SECULAR PERIOD ANALYSIS

A combination of photographic, photoelectric and ccd-derived times-of minimum published between 1978 and 2022 are summarized in Table 1. An eclipse timing difference (ETD) plot (aka "O-C diagram") was initially seeded using the eclipse elements taken from the International Variable Star Index (`https://www.aavso.org/vsx/index.php?view=detail.top\&oid=186067`). After updating the linear ephemeris (Equation 1) using near-term (2017-2021) timings it was apparent that a change in the ETD residuals could be established (Fig. 1) that was best fit with a quadratic expression (Equation 2).

$$MinI(HJD) = 2\ 459\ 363.7562(7) + 0.5294714(5) \cdot E \tag{1}$$

$$ETD = 0.00416 \pm 1.3000 \cdot 10^{-3} + 1.5397 \pm 2.4283 \cdot 10^{-7} E - 1.3457 \pm 0.0883 \cdot 10^{-10} E^2\ . \tag{2}$$

Since the quadratic term coefficient (Q=-1.3457 $\pm$ 0.0883) is negative, this result would suggest that the orbital period has been decreasing at the rate:

$$dP/dt = 2Q/P = 0.016 \pm 0.001\ s \cdot y^{-1}. \tag{3}$$

Period change defined by a parabolic relationship is often attributed to angular momentum loss (AML) due to magnetic stellar wind or by mass transfer (Stępień 1995; Stępień 2006; Qian 2001, 2003; Li et al. 2019). Ideally the net effect is a decreasing orbital period when AML dominates. The orbital period can also decrease when conservative mass transfer from the more massive to its less massive binary partner is the dominant process. In contrast, separation of the binary pair increases when conservative mass transfer from the less massive to its more massive cohort occurs or when spherically symmetric mass loss from either body (e.g. a wind but not magnetized) takes place. In mixed

situations (e.g. mass transfer from less massive star, together with AML) the orbit evolution depends on which process prevails (Alton & Stępień 2018).

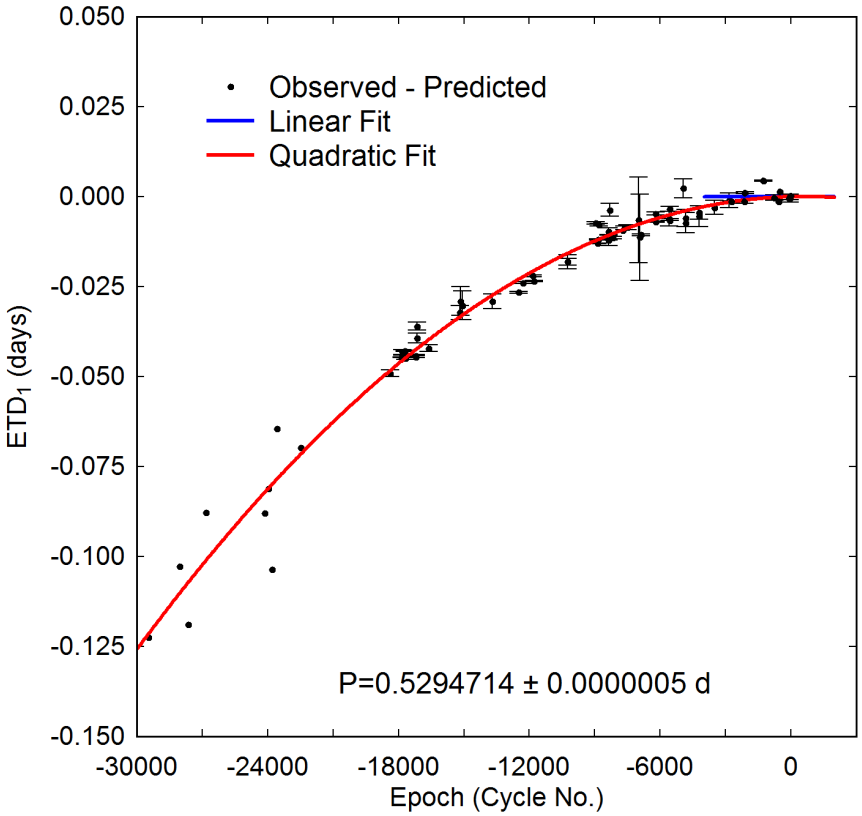

Fig. 1. V878 Her: Eclipse timing difference (ETD) plot generated using the eclipse elements from Equation 1. Significant scatter observed during earlier epochs is attributed to ToM values estimated from photographic plates.

3. EFFECTIVE TEMPERATURE ESTIMATION

Interstellar extinction was estimated using the dust maps originally generated by Schlegel et al. (1998) and then later adjusted by Schlafly & Finkbeiner (2011). A mean value for $T_{\rm eff1}$ (6300 ± 138 K) was adopted from multiple surveys including 2MASS (6272 K) using J, K and H transforms to the Johnson-Cousins photometric system (Warner 2007), Gaia DR2 (6274 K), Gaia DR3 (6262 K), UCAC4 (6175 K), TESS (6181 K) and that estimated from $(V\text{-}R_c)_o$ at MAO (6440 K). Accordingly, the spectral type of the primary star would likely range between F6 and F7, or close to F8 as reported by Ren et al. (2020).

TABLE 1

V878 HER TIMES OF MINIMUM (ToM), MEASUREMENT UNCERTAINTY, EPOCH AND ECLIPSE TIMING DIFFERENCES (ETD) USED TO CALCULATE LINEAR AND QUADRATIC EPHEMERIDES.

ToM (HJD-2400000)	Err	Cycle No.	ETD	Ref.	ToM (HJD-2400000)	Err	Cycle No.	ETD	Ref.
43759.5820	nr	-29471	-0.1224	1	54932.5981	0.0002	-8369	-0.0119	14
44512.5100	nr	-28049	-0.1027	1	54933.3945	0.0010	-8367.5	-0.0097	14
44733.8130	nr	-27631	-0.1188	1	54971.5224	0.0018	-8295.5	-0.0037	14
45161.6570	nr	-26823	-0.0877	1	55045.3760	0.0004	-8156	-0.0114	15
46590.7000	nr	-24124	-0.0880	1	55275.1686	0.0000	-7722	-0.0094	16
46669.5980	nr	-23975	-0.0812	1	55321.7629	0.0005	-7634	-0.0086	17
46757.4680	nr	-23809	-0.1035	1	55396.4184	0.0006	-7493	-0.0085	15
46879.8150	nr	-23578	-0.0644	1	55662.4798	0.0119	-6990.5	-0.0065	18
47466.4640	nr	-22470	-0.0697	1	55695.5670	0.0120	-6928	-0.0113	19
49637.5821	0.0009	-18369.5	-0.0491	1	55725.7476	0.0003	-6871	-0.0106	20
49917.6769	0.0001	-17840.5	-0.0447	1	56077.3202	0.0002	-6207	-0.0070	21
49922.7073	0.0002	-17831	-0.0443	1	56082.3525	0.0004	-6197.5	-0.0047	21
49927.7383	0.0006	-17821.5	-0.0432	1	56398.9750	0.0020	-5599.5	-0.0061	22
49983.5979	0.0002	-17716	-0.0429	1	56416.1822	0.0000	-5567	-0.0067	23
50001.5979	0.0003	-17682	-0.0449	1	56418.8298	0.0002	-5562	-0.0064	22
50251.5088	0.0003	-17210	-0.0445	2	56422.8038	0.0006	-5554.5	-0.0034	22
50251.5090	0.0004	-17210	-0.0443	2	56750.5524	0.0026	-4935.5	0.0023	24
50291.4891	0.0014	-17134.5	-0.0393	2	56799.5203	0.0024	-4843	-0.0059	24
50291.4924	0.0011	-17134.5	-0.0360	2	56808.5199	0.0028	-4826	-0.0073	24
50573.4298	0.0009	-16602	-0.0421	3	57131.5003	0.0019	-4216	-0.0044	25
51323.4360	0.0020	-15185.5	-0.0322	4	57137.5883	0.0029	-4204.5	-0.0054	25
51338.7938	0.0040	-15156.5	-0.0290	5	57499.4844	0.0019	-3521	-0.0030	25
51386.4451	0.0040	-15066.5	-0.0302	4	57855.5559	0.0021	-2848.5	-0.0010	26
52118.4404	0.0020	-13684	-0.0291	6	57915.6505	0.0002	-2735	-0.0014	27
52743.7486	0.0003	-12503	-0.0266	7	58228.5682	0.0005	-2144	-0.0013	28
52859.1761	0.0002	-12285	-0.0239	8	58246.8374	0.0002	-2109.5	0.0011	29
53088.9686	0.0002	-11851	-0.0220	9	58688.4198	0.0002	-1275.5	0.0044	30
53115.4406	0.0002	-11801	-0.0235	8	58962.4166	0.0008	-758	-0.0003	31
53932.4204	0.0009	-10258	-0.0181	10	59061.4267	0.0000	-571	-0.0013	32
53941.4214	0.0019	-10241	-0.0181	11	59069.3688	0.0000	-556	-0.0013	32
54628.4214	0.0003	-8943.5	-0.0073	12	59090.0208	0.0000	-517	0.0013	32
54669.4497	0.0001	-8866	-0.0130	13	59321.3980	0.0010	-80	-0.0005	33
54683.4818	0.0002	-8839.5	-0.0119	13	59330.3990	0.0010	-63	-0.0005	33
54701.4879	0.0003	-8805.5	-0.0078	13	59330.3994	0.0007	-63	-0.0001	34
54928.3621	0.0015	-8377	-0.0121	14	59363.7563	0.0003	0	0.0001	35

nr: not reported

1. Kaiser et al. (1996); 2. Agerer & Huebscher (1997); 3. Agerer & Hübscher (1999); 4. Agerer et al. (2001)
5. Bloomer & Ngwele (1999); 6. Agerer & Hübscher (2002); 7. Dvorak (2004); 8. Krajci (2005)
9. Nelson (2005); 10. Hübscher et al. (2006); 11. Hübscher & Walter (2006); 12. Bràt et al. (2008)
13. Yilmaz et al. (2009); 14. Hübscher et al. (2010); 15. Hübscher & Monninger (2011); 16. Nagai (2011)
17. Diethelm (2010); 18. Hübscher et al. (2012); 19. Paschke (2011); 20. Diethelm (2011)
21. Liakos et al. (2014); 22. Nelson (2014); 23. Nagai (2014); 24. Hübscher & Lehmann (2015)
25. Hübscher (2017); 28. Pagel (2018b); 26. Pagel (2018a); 27. Samolyk (2017)
29. Nelson (2019); 30. Pagel (2020); 31. Pagel (2021); 32. Nagai (2021)
33. Paschke (2021); 34. Pagel (2022); 35. Nelson (2022)

TABLE 2

V878 HER AND THREE COMPARISON STARS USED FOR ENSEMBLE APERTURE PHOTOMETRY.

Object	RA (J2000)	Dec (J2000)	V-mag	(B-V)
V878 Her	17:24:25.278	+49:38:37.26	9.92	0.522
GSC 3516-0810	17:25:40.521	+49:33:25.70	10.32	1.18
GSC 3516-0710	17:25:57.766	+49:33:27.00	10.62	1.13
GSC 3516-0361	17:26:03.191	+49:35:47.90	11.28	0.979

4. PHOTOMETRIC OBSERVATIONS

Between April 16, 2013 and May 7, 2014 a total of 277 science frames in V, 276 in R_c and 276 in the I_c passbands were taken at Mountain Ash Observatory (MAO) in Prince George, BC, Canada. The imaging equipment included a 33-cm $f/4.5$ Newtonian telescope coupled with an SBIG ST-10XME ccd camera which were installed on a Paramount ME mount. Image calibration was performed using standard dark subtraction and flat fielding (CCDSoft Version 5.00.210). Three comparison stars used during ensemble aperture photometry (MPO Canopus v10.7.12.9) are listed in Table 1 along with their J2000 coordinates (Gaia EDR3; Gaia Collaboration (2021)) and magnitudes (APASS-DR9; Henden et al. (2009)). Comparison star differences were constant to within ∼0.01 magnitude, with no apparent systematic variation.

Primarily designed to detect very small brightness changes from a host star during an exoplanet transit, the TESS Mission (Ricker et al. 2015; Caldwell 2020) also provides a rich source of light curve data for many more traditional variable stars. The TESS CCD detector bandpass ranges between 600-1000 nm and is centered near Cousins I band (I_c). The first imaging campaign in the vicinity of V878 Her started on April 16, 2020 and ran every 2 min through May 12, 2020. Another group of images were then similarly acquired between May 14, 2020 and June 8, 2020. Since light curves from this second group exhibited some obvious changes in amplitude (probably due to change in spot size or location) we chose to only evaluate those light curve data acquired between April 16 and May 12, 2020. Raw flux readings were processed by the TESS Science Processing Operations Center (TESS-SPOC) to remove long term trends using so-called Co-trending Basis Vectors (CBVs). These results identified as "Pre-search Data Conditioning Simple Aperture Photometry" (PDCSAP) flux are usually cleaner data than the SAP flux.

5. SPECTROSCOPIC OBSERVATIONS

Starting in April, 2009 and ending on August 29, 2020 a total of 22 medium-resolution (R∼10,000) spectra were acquired at the Dominion Astrophysical Observatory (DAO) in Victoria, British Columbia, Canada using

TABLE 3

LOG OF DAO OBSERVATIONS AND RESULTS.

Mid-time HJD-2400000	Exposure (s)	Phase at Mid-exp	RV_1 ($km \cdot s^{-1}$)	RV_1 err ($km \cdot s^{-1}$)	RV_2 ($km \cdot s^{-1}$)	RV_2 err ($km \cdot s^{-1}$)
54925.8980	2400	0.361	-115.64	6.5	112.09	11.21
54927.8954	2498	0.134	-90.74	6.15	135.92	9.75
54927.9435	3600	0.225	-114.84	6.73	173.48	15.07
54927.9977	3600	0.327	-99.92	3.54	143.95	9.29
55668.9429	1800	0.730	65.10	3.98	-240.85	3.35
56403.8551	1940	0.738	57.26	12.5	-240.28	9.53
56404.9559	3600	0.817	73.29	6.91	-251.13	18.24
56405.9400	3600	0.676	55.75	3.95	-222.60	3.2
56407.8898	3600	0.358	-119.12	2.13	147.51	4.71
56761.0290	1235	0.323	-150.64	3.79	179.61	3.1
56765.9727	3600	0.660	55.16	5.88	-219.35	11.02
56766.0108	2799	0.732	66.25	3.93	-244.69	2.27
57493.9813	1800	0.630	30.26	2.31	-193.36	3.3
57504.8839	720	0.221	-117.84	3.41	147.36	6.7
57504.9509	700	0.348	-125.42	13.64	57.81	11.45
57995.7647	700	0.334	-127.71	3.51	138.97	6.65
58008.7406	700	0.841	67.19	3.65	-243.50	2.27
58234.0069	700	0.296	-132.41	8.64	180.19	5.98
58241.9784	700	0.351	-121.90	2.25	153.16	5.98
58241.9870	700	0.367	-108.80	5.88	150.16	11.25
58597.9718	700	0.706	71.14	9.79	-224.91	8.88
59100.7570	700	0.303	-102.86	3.46	168.78	5.84

the 1.83-m Plaskett Telescope. The spectrograph, fitted with a 2118Yb grating (1800 lines/mm and blazed at 500 Angstroms), produced a reciprocal dispersion approximating 10 Å/mm. The wavelength range (5000 to 5250 Å) was chosen to include the strong iron absorption lines at 5167.48 and 5171.59 Å. Spectra from an iron-argon lamp taken immediately before and after each stellar spectra were used for wavelength calibration. RV standard stars were selected from the 1986 Astronomical Almanac (Section H42-2), many of which were also listed as suitable IAU radial velocity standard stars (Stefanik et al. 1999). These have been proven to be extremely reliable and consistent with the results achieved in over 20 publications using the same 1.83-m Plaskett Telescope. In general, stars were selected near in spectral type (and luminosity class) to the target stars (typically A-F, luminosity class V) and as bright as possible. Typical exposures of standards (running from magnitude 2.0 to 8.0) on a 1.5-2 meter class optical telescope run from a few seconds to perhaps 10 or 20 min. Windows software RaVeRe, written by the first author, and available on his website (Nelson 2013), was used for de-trending and reduction of the spectral data. The radial velocities were determined by the Broadening Functions (BF) routine (Ruciński (1969); Ruciński (1992); Ruciński (2004); Nelson (2010)) as implemented in the Windows-based application Broad (Nelson 2013); details regarding this procedure are provided in Nelson (2010). The elements used for all phasing are given in Equation 1. A log of observations ($RV_{1,2}$) corrected for Heliocentric Julian Date (HJD) are presented in Table 2; each RV uncertainty estimate is derived from the standard deviation of values from multiple comparison stars. The calibrated one-dimensional spectra, sorted by phase, are presented in Figure 2. To disentangle the components, Gaussian profile curve fitting was employed according to Nelson (2020). Representative broadening peaks are illustrated at phase 0.323 (Figure 3) and phase 0.706 (Figure 4).

6. LIGHT CURVE ANALYSES

V878 Her light curve morphology is consistent with eclipsing variables identified as near contact binary stars (NCBs). Shaw (1994) classified these systems based upon their short orbital periods (<1 d), tidal interactions, and facing surfaces that are less than 0.1 orbital radii apart. Light curves from some semi-detached classical Algols and β Lyrae type eclipsing binary systems appear similar to those exhibited by NCBs. However, one distinguishing difference is the effective temperature (T_{eff}) of the more massive component defined herein as the primary star. Compared to NCBs which typically feature a late F spectral type component along with a cooler (G-K spectral type) companion, β Lyrae and Algol-like binaries usually include at least one massive (O, B and A spectral type) consituent. Depending on the evolutionary status of each pair, Roche lobe overflow (RLOF) in all three cases may lead to mass transfer by the donor and mass gain by the accretor.

Roche-lobe modeling of light curve data acquired at MAO (Figure 5) and TESS (Figure 6) was initially performed with *PHOEBE* 0.31a (Prša & Zwit-

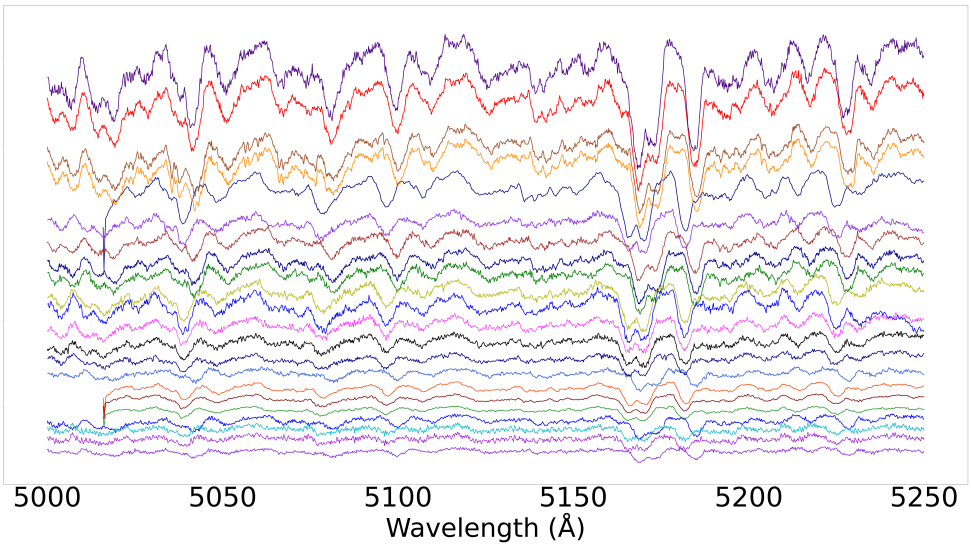

Fig. 2. V878 Her spectra sorted by phase (Table 3) and offset for clarity. The vertical scale is arbitrary.

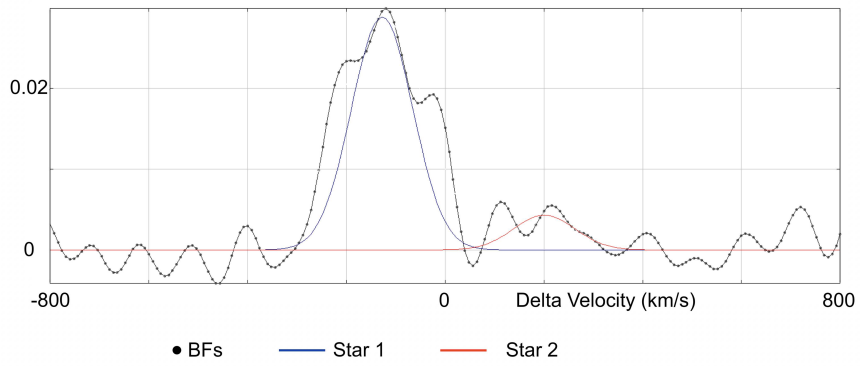

Fig. 3. Broadening function for V878 Her at phase 0.323 and the fitted Gaussian profiles. The standard spectrum is from HD 126053 while the target spectrum was the mid-value (n=7) obtained on HJD 2456761.0290.

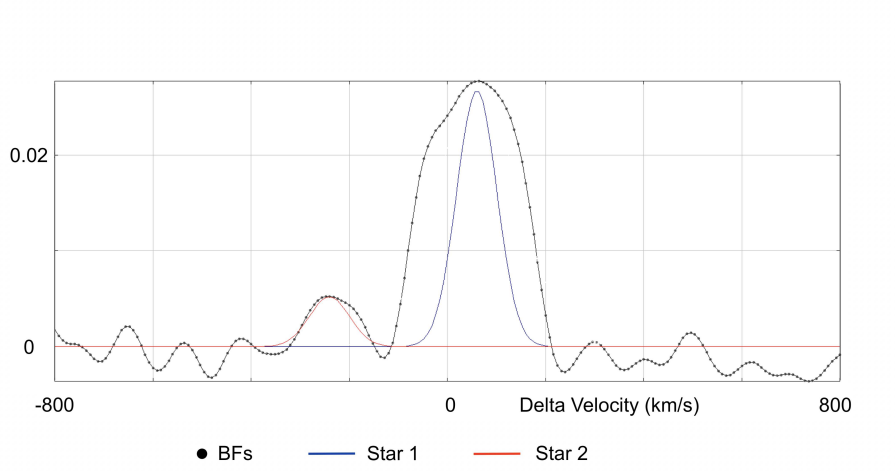

Fig. 4. Broadening function for V878 Her at phase 0.706 and the fitted Gaussian profiles. The standard spectrum is from HD 126053 whereas the program spectrum was the mid-value (n=5) acquired on HJD 2458597.9718.

ter 2005) and then refined using *WDwint56a* (Nelson 2009). Both programs feature a graphical interface to the Wilson-Devinney WD2003 code (Wilson & Devinney 1971; Wilson 1979, 1990). *WDwint56a* incorporates Kurucz's atmosphere models (Kurucz 1993) that are integrated over VR_cI_c passbands. Based on the assumption that V878 Her is an NCB system, Roche-lobe modeling proceeded using Mode 5 for an Algol-like semi-detached binary where the secondary star fills the Roche lobe. Other modes (overcontact and semi-detached with primary star filling the Roche lobe) never improved light curve simulation as defined by the model residual mean square errors. Since the effective temperature of the primary was estimated to be 6300 K, internal energy transfer to the stellar surface is driven by convective (<7200 K) rather than by radiative processes (Bradstreet & Steelman 2004). Therefore, bolometric albedo ($A_{1,2}$=0.5) was assigned according to Ruciński (1969) while the gravity darkening coefficient ($g_{1,2}$=0.32) was adopted from Lucy (1967). Logarithmic limb darkening coefficients (x_1, x_2, y_1, y_2) were interpolated (van Hamme 1993) following any change in effective temperature during model fit optimization by differential corrections (DC). All but the temperature of the more massive star (T_{eff1}), $A_{1,2}$ and $g_{1,2}$ were allowed to vary during DC iterations. In general, the best fits for T_{eff2}, i, q and Roche potentials (Ω_1, Ω_2) were collectively refined (method of multiple subsets) by DC using the multi-bandpass light curve data until a simultaneous solution was found. It should be noted that V878 Her did not require any third light correction (l_3=0) to improve W-D model fits. Light curve data acquired at MAO between 2013 and 2014 (Figure 5) and from the TESS satellite (Figure 6) in 2020 exhibited obvious asymmetry during quadrature (Max I>Max II). This so-called "O'Connell effect" (O'Connell 1951), posits the presence of a star spot leading to surface

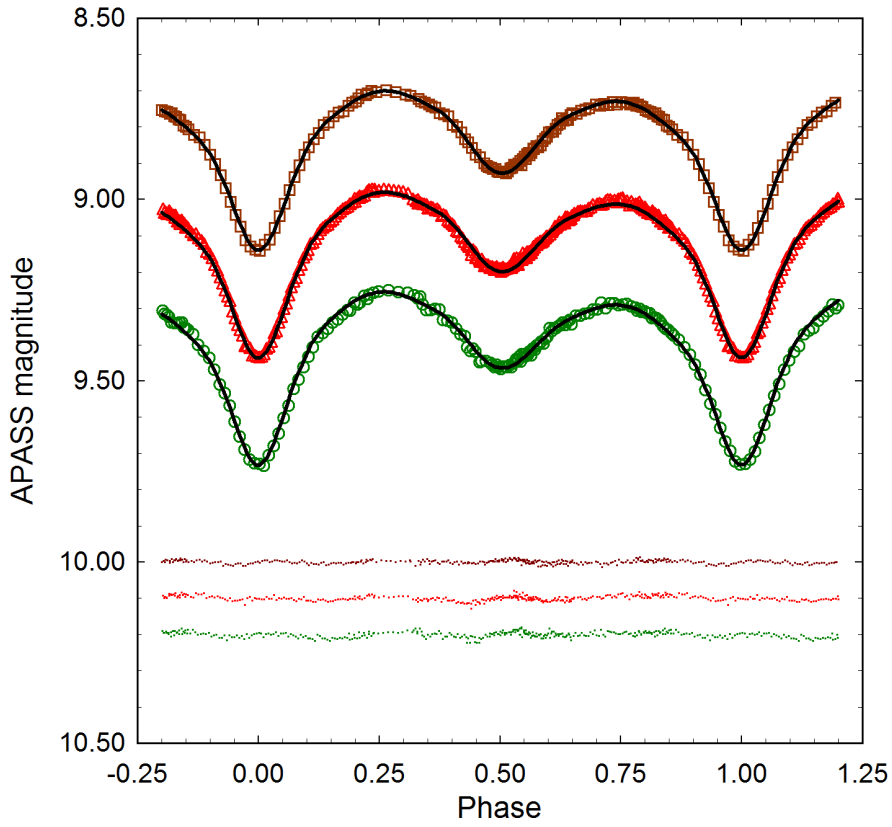

Fig. 5. V878 Her light curves from MAO (2013-2014) superimposed with W-D Roche model simulations (solid black lines). Plotted are, top to bottom: I_c, R_c and V. At the bottom of the figure, the model fit residuals are provided in the same order as the light curves.

inhomogeneity. In this case the addition of a large hot spot positioned near the neck region of the secondary star provided the best fit light curve simulations. This persistent feature found in light curves acquired between 2013-2020 is consistent with magnetospheric accretion resulting from mass transfer onto the secondary star and the predicted orbital period decrease over time. The properties of V878 Her position this star into the category of SD1 binaries. Detection of X-rays coincident with the location of V878 Her (Norton 2007) suggests that the high energy physics normally associated with mass transfer in an NCB (Shaw 1994) is consistent with the putative location of a hot spot in the neck region. Final models using the TESS and land-based light curves provided similar effective temperatures for the secondary where T_{eff2}=4243 and 4391 K, respectively. These values correspond more closely to spectral class K5-K6 (Pecaut & Mamajek 2013).

The remaining W-D model fit parameters from the MAO and TESS datasets (Table 3), differ only slightly including the spot size and location which might

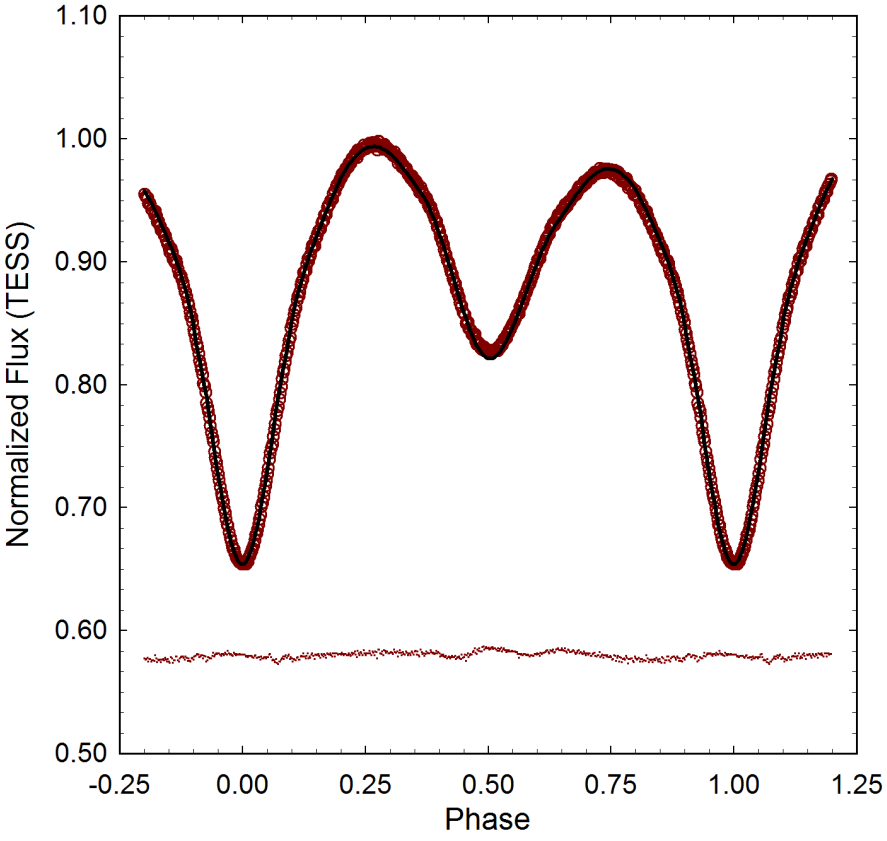

Fig. 6. Peak normalized V878 Her light curve and the Roche lobe modeling results from the TESS Mission (April 16–May 12, 2020). At the bottom of the figure, the differences between the observed and simulated light curve fits are plotted with a fixed offset (0.4).

be expected to change in the time interval between the two datasets. If we assume the hot spot on the secondary star results from conservative mass transfer, the amount of material lost by the donor primary can be estimated according to Kwee (1958):

$$dm/dt = m\Big[\frac{q}{3P(1-q^2)}\Big]dP/dt. \quad (4)$$

where

$$m = M_1 + M_2 \; and \; q = M_2/M_1. \quad (5)$$

Based on the combined mass of the primary (1.55 $M_\odot$) and secondary (0.69 $M_\odot$) stars (Table 4), conservative mass transfer is estimated to be $1.44 \pm 0.129{\cdot}10^{-7}$ $M_\odot{\cdot}y^{-1}$. This value falls well within the range (0.13-2.79$\cdot 10^{-7}$ $M_\odot{\cdot}y^{-1}$) reported by Zhu et al. (2009) for other NCBs of SD1 type. Assuming that accretion onto the secondary was continuous between 1978 and 2021 (Table 2), nearly 2.1 times the Earth's mass was transferred.

7. SPECTROSCOPIC ANALYSES

Stand alone radial velocity observations fit with a sine curve model are plotted in Fig. 7 and yielded the following values: K_1 = -101.7 $\pm$4.3 km$\cdot$s^{-1}, $K_2 = 219.5 \pm 2.4$ km$\cdot$s^{-1}, RV_γ = -34.4 $\pm$ 5.0 km$\cdot$s^{-1}(systemic velocity). When modeled without any light curve data, the spectroscopic mass ratio (q_{sp}=M_2/M_1) was determined to be 0.464 $\pm$ 0.040. Given the inherent precision of the TESS satellite-based photometric observations, we adopted the physical and geometric parameters obtained following simultaneous Roche-type light curve modeling (WD2003) with the RV data. This produced the following estimates for M_1 (1.55 ± 0.18 $M_\odot$), M_2 (0.69 ± 0.23 $M_\odot$), R_1 (1.62 ± 0.03 $R_\odot$), R_2 (1.12 ± 0.02 $R_\odot$), q_{WD}=0.442 ± 0.001, L_1 (3.75 ± 0.36 $L_\odot$), and L_2 (0.37 ± 0.04 $L_\odot$). The mass ratio (0.442 ± 0.001) derived from modeling the combined curves (RV+TESS-LC) is negligibly different from the spectroscopically determined mass ratio (0.443 ± 0.002) calculated from the multi-bandpass (VR_cI_c) light curves acquired at MAO.

In the present dataset, each RV estimate is the mean of values obtained from eight different standards; uncertainty is simply the standard deviation of the group. WD2003 parameter values with associated uncertainty following Roche-lobe modeling are listed in Table 3. These are formal statistical values known to be smaller than total uncertainty since systematic experimental errors can not be readily determined. Spatial representations of V878 Her rendered with Binary Maker 3 (Bradstreet & Steelman 2004) are illustrated in Fig. 8.

8. EVOLUTIONARY ANALYSIS OF V878 HER

8.1. *General considerations*

Evolutionary status of NCBs has been a matter of debate since their identification as a separate group of variables, particularly in connection with

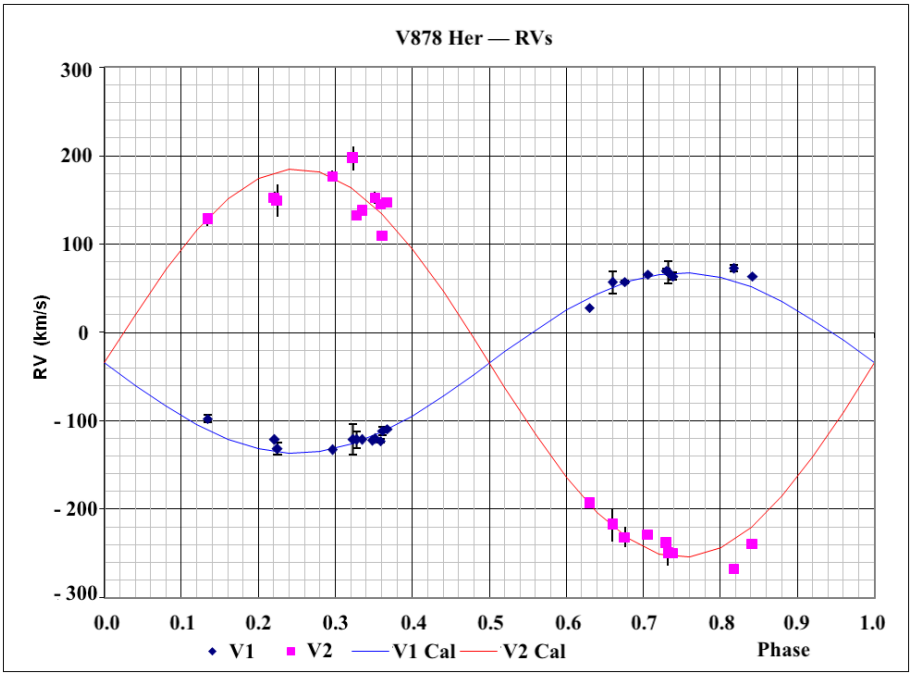

Fig. 7. Observed V878 Her radial velocities with W-D solution using photometric data from the TESS Mission. Since the computed curves from the MAO and TESS datasets were visually identical, only one RV plot is presented.

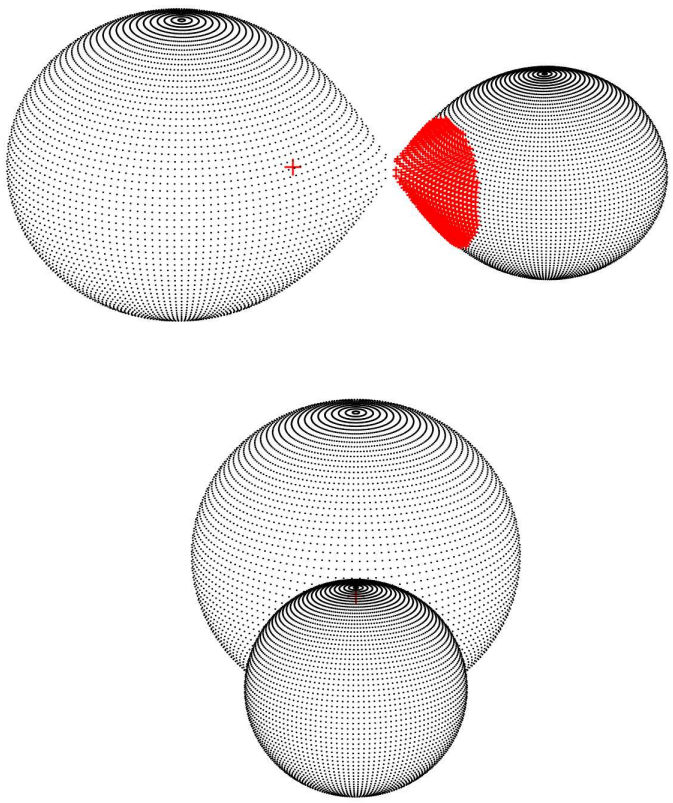

Fig. 8. Roche surface potentials and spatial representations of V878 Her from the TESS mission (April 16–May 12, 2020). The hot spot (top) located in the neck region showed little sign of changing between 2013 and 2020 suggesting a sustained period of mass transfer and accretion onto the secondary star. This is consistent with the orbital period secular analysis (Fig. 1). The bottom figure depicts the partial eclipse (i$\simeq$69°) as seen from our vantage point

TABLE 4

WILSON-DEVINNEY PARAMETERS FOR THE BEST-FIT V878 HER LIGHT CURVE SOLUTION

WD Quantity[a]	TESS	MAO
T_{eff1} (K)[b]	6300 (138)	6300 (138)
T_{eff2} (K)	4243 (93)	4391 (96)
q (m_2/m_1)	0.442 (1)	0.443 (2)
Ω_1	2.763 (1)	2.766 (4)
Ω_2	2.763 (1)	2.766 (4)
i°	69.05 (3)	68.75 (16)
a ($R_\odot$)	3.60 (7)	3.51 (07)
V_γ (km·s^{-1})	-29.4 (1.7)	-29.2 (1.3)
$A_S = T_S/T_\star$[c]	1.18 (1)	1.17 (1)
Θ_S(spot co-latitude)[c]	89.6 (4)	93.9 (1.8)
ϕ_S (spot longitude)[c]	23.2 (8)	47.3 (1.6)
r_S (angular radius)[c]	34.3 (2)	34.5 (7)
$L_1/(L_1+L_2)_V$[d]	···	0.940 (1)
$L_1/(L_1+L_2)_{R_c}$	···	0.915 (1)
$L_1/(L_1+L_2)_{I_c}$	···	0.894 (1)
$L_1/(L_1+L_2)_{TESS,\ I_c}$	0.911 (11)	···
r_1 (pole)	0.4244 (1)	0.4241 (8)
r_1 (point)	0.5820 (342)	0.5739 (209)
r_1 (side)	0.4591 (2)	0.4515 (10)
r_1 (back)	0.4793 (2)	0.4788 (12)
r_2 (pole)	0.2902 (1)	0.2904 (1)
r_2 (point)	0.4170 (1)	0.4172 (1)
r_2 (side)	0.3027 (1)	0.3029 (1)
r_2 (back)	0.3353 (1)	0.3355 (1)

[a]All uncertainty estimates for q, $\Omega_{1,2}$, i, $r_{1,2}$, and L_1 from *WDwint56a* (Nelson 2013)

[b]Fixed with no error during DC

[c]Secondary spot parameters in degrees (Θ_P, ϕ_P and r_P); A_P equals the spot temperature (T_S) divided by star temperature, T_*

[d]L_1 and L_2 refer to scaled luminosities of the primary and secondary stars, respectively

W UMa type binaries. Lucy (1976) developed a model of a cool contact binary in which both components oscillate around a marginal thermal equilibrium remaining in contact for a part of the cycle and in a semidetached

configuration for the rest. The model was called Thermal Relaxation Oscillations (TRO) theory. Following the theory, candidates for the broken contact binaries were sought and SD1 binaries seemed to be natural choice (Lucy & Wilson 1979; Eggleton 2006). However, several authors considered these binaries as "first timers" i.e. semidetached binaries that are coming into first-time contact (Shaw 1994; Hilditch et al. 1998). Others noticed several problems with SD1 binaries being TRO oscillators, like a systematic difference between masses and angular momenta of SD1 and W UMa binaries. Some suggested that only a fraction of SD1 binaries can be first timers while the others are TRO oscillatiors. The problem then arises how to distinguish one from another (van Hamme et al. 2001; Yakut & Eggleton 2005).

A thorough discussion of the properties of NCBs of both groups and a comparison with W UMa type binaries was carried out by Stępień & Kiraga (2013). The authors demonstrated that not only the mean values of period, component masses and angular momentum but also their distributions are distinctly different from the corresponding features of W UMa stars. In contrast, the distributions of both groups of NCBs, i.e. SD1 and SD2, are similar to each other indicating generic connection between them. In conclusion the authors support the early hypothesis developed by Shaw (1994) according to which SD1 binaries are formed from close detached binaries when the more massive binary fills its critical Roche lobe and transfers matter to the secondary until the original secondary becomes a more massive component, passing through the contact configuration. The mass transfer still goes on and the binary assumes an SD2 configuration. Later, an A type W UMa binary or short period Algol is formed depending on the amount of angular momentum left in the system. In considering the evolution of the progenitor of V878 Her we adopt the above scenario.

If SD1 binaries cannot be considered as TRO oscillators, the basic prediction of the theory is not confirmed. In fact, even assuming that SD1 *are* TRO oscillators, they can explain only the most massive and the longest period tails of W UMa star distributions. An overwhelming majority of W UMa stars have periods, masses and angular momenta substantially lower than SD1 binaries and we do not observe any semi-detached binaries within these ranges.

To solve the problem, an alternative evolutionary model of cool contact binaries has been developed by one of us (Stępień 2006, 2009, 2011). The model assumes that the binaries are past mass transfer in case A (Kippenhahn & Weigert 1967) with the mass ratio reversal and each component separately remains in thermal equilibrium. The present secondary is the more advanced evolutionary former primary and the present primary is very little evolved former secondary which gained hydrogen rich matter from its companion. The evolution of the progenitor of a contact binary can be divided into three phases: an initial detached binary tightens its orbit due to the angular momentum loss via a magnetic wind and at the same time the more massive component expands evolutionary. The first phase comes to end when the primary fills its Roche lobe and starts transferring matter to its companion. The

second phase correspond to the rapid mass transfer until mass ratio reversal and the third phase describes a final evolution of a binary until coalescence of both components. The basic assumptions and equations of the model, i.e. the expression for binary angular momentum, Kepler's Third Law, the approximate expression for Roche-lobe sizes, as well as those describing mass and angular momentum losses due to the magnetized wind are described elsewhere (Stępień et al. 2017). Evolutionary models of single stars PARSEC (Bressan et al. 2012) are used to approximate the evolution of both components at each time step. While this approximation is satisfactory for the first and third phase when each component is in thermal equilibrium, it is poorly satisfied during the rapid mass exchange when both components are out of thermal equilirium. Unfortunately, SD1 binaries seem to be exactly in this phase, as observations indicate, which means that the computed values of the stellar parameters during that phase should be treated as approximate.

A series of evolutionary models for V878 Her progenitors has been calculated from zero-age main sequence (ZAMS) through the Roche lobe overflow (RLOF) till the near contact phase. Details of the mass transfer following RLOF are described by Stępień & Kiraga (2013). Right after RLOF the more massive component transfers mass on its thermal time scale or even faster, depending on values of the binary parameters (Sarna & Fedorova 1989; Ge et al. 2010). After about 0.1 $M_\odot$ is transferred, the secondary swells and approaches its Roche lobe. When its radius is very close to the size of the Roche lobe, the secondary does not accept all trasferred mass and a fraction of this matter returns to the primary after encircling the secondary. The mass transfer rate drops and is determined now by the rate at which the secondary tends to shrink trying to regain thermal equilibrium.

We assume that V878 Her is just in the phase when the secondary approaches its Roche lobe. In result we stop calculations when 0.1 $M_\odot$ is transferred to the secondary past RLOF.

8.2. *Results of calculations*

NCBs present a serious difficulty for spectroscopic observations. As Shaw (1994) noted, contrary to contact systems where comparable surface brightnesses of both components result in a moderate contrast of their luminosities, a substantial difference in temperatures of NCB components makes this contrast reach a factor of the order of 10 or even 100. This is why so few NCBs have measured radial velocity curves and quite often with a rather low accuracy. This is also the case of V878 Her that results in significant uncertainties of the observed values of the component masses. To allow for this uncertainty we computed a series of models with masses from the range given by error limits.

Our basic model is supposed to reproduce the best estimates of masses $M_1 = 1.55 M_\odot$ and $M_2 = 0.69 M_\odot$ together with orbital parameters as given in Table 4. Its initial, ZAMS values turned out to be $M_1 = 1.659 M_\odot$, $M_2 = 0.597 M_\odot$ and $P = 1.57$ day. After 1.26 Gyr the more massive component

reaches RLOF and the binary parameters are as follows: $M_1 = 1.645 M_\odot$, $M_2 = 0.594 M_\odot$, $R_1 = 2.051 R_\odot$, $R_1 = 0.578 M_\odot$ and $P = 0.708$ day. The radius of the primary at this moment expanded to 0.65 of the value reached by a star of this mass at the terminal main sequence. The secondary is still very little evolved so its radius is close to its ZAMS value. The core luminosities of both stars are $L_1 \approx 11 L_\odot$ and $L_2 \approx 0.07 L_\odot$. After additional 10^7 years about 0.1 $M_\odot$ is transferred from the primary to the secondary. The resulting parameters are now: $M_1 = 1.545 M_\odot$, $M_2 = 0.694 M_\odot$ and $P = 0.529$ day. The values of stellar radii resulting directly from the computations are unreliable because the calculations do not allow for deviations from thermal equilibrium so we simply assume that they are close to radii of both Roche lobes, i.e. $R_1 \approx 1.62 R_\odot$ and $R_2 \approx 1.12 R_\odot$. The core luminosities are not expected to change significantly compared to the RLOF phase as the rapid mass transfer hardly influences the interior of stars. Note that they differ significantly from the presently observed values $L_1 \approx 3.75 L_\odot$ $L_2 \approx 0.37 L_\odot$. It is so because a fraction of the core luminosity of the primary is converted into the potential energy of expanding layers and also transferred to the secondary.

When calculating models with masses deviating from the best adopted values by one standard error we kept the orbital period and mass ratio fixed. Both quantities are determined with sufficiently high accuracy to neglect their possible deviations. This, together with the requirement that both masses are within one error from the adopted values means that the minimum component masses are $M_1 = 1.37 M_\odot, M_2 = 0.61 M_\odot$ and the maximum allowed masses are $M_1 = 1.73 M_\odot, M_2 = 0.76 M_\odot$. The low mass model is reproduced satisfactorily by an initial ZAMS binary with $M_1 = 1.49 M_\odot, M_2 = 0.51 M_\odot$ and $P = 1.95$ day. After 1.8 Gyr the primary fills its Roche lobe and RLOF begins with the following binary parameters: $M_1 = 1.472 M_\odot, M_2 = 0.505 M_\odot$, $P = 0.752$ day, and after another 10^7 years the model binary resembles the present variable with the parameters $M_1 = 1.367 M_\odot, M_2 = 0.60 M_\odot$, $P = 0.527$ day. Similarly, the ZAMS high mass model has $M_1 = 1.835 M_\odot, M_2 = 0.670 M_\odot$, $P = 1.28$ day, after 8.5×10^8 years at the RLOF the masses and the orbital period are $M_1 = 1.826 M_\odot, M_2 = 0.666 M_\odot$, $P = 0.670$ day, whereas after additional 10^7 years these values are $M_1 = 1.733 M_\odot, M_2 = 0.759 M_\odot$, $P = 0.530$ day.

It follows from the model computations that a progenitor of V878 Her was a detached binary with the initial period of 1.5 day (possibly, between 1.3 and 2 days),in a good agreement with the results of Stępień (2011) who argued that the initial (ZAMS) binary period distribution has a cut-off around 1.5-2 days. The initial mass ratio was $q_{init} = 0.36$ (0.34 or 0.37 for the minimum and maximum mass models, respectively). Mass transfer began at RLOF when the primary radius was equal to about 2/3 of the TAMS radius and the binary was about 1 Gyr old. The primary was massive enough to have a radiative envelope hence the mass transfer to the secondary made its radius shrink. However, the low value of q resulted in even stronger shrinking of the primary's Roche lobe. In effect, the mass transfer rate should have quickly risen from

thermal to dynamical (Sarna & Fedorova 1989; Nelson & Eggleton 2001; Ge et al. 2010) until the secondary fills its Roche lobe. But the observations show the opposite: while the theoretical thermal rate at RLOF, given by $\dot{M}_{th} = 3.3 \times 10^{-8} RL/M = 4.7 \times 10^{-7}\ M_{\odot}$/year, the observed rate is equal to only $1.44 \times 10^{-7}\ M_{\odot}$/year, i.e. three times lower. The expected thermal mass transfer rate is somewhat lower after 0.1 of the solar mass has been transferred but it is still significantly higher than observed, not to mention about the dynamical rate which is orders of magnitude higher. The low observed mass transfer rate supports the evolutionary model of the mass transfer presented by Stępień & Kiraga (2013) that assumes that in the late phase of rapid mass transfer, when the secondary is almost touching its Roche lobe, the net mass transfer rate decreases as the increasing fraction of the mass flux returns to the primary. The secondary ultimately accepts matter at the rate dictated by its thermal time scale after a contact system is formed.

Figure 9 shows the positions of both components from V878 Her on the HR diagram, as compared to other NCBs of SD1-type analysed in a recent paper by Tian & Chang (2020). It should be stressed, however, that the apparent temperatures and luminosities of NCBs do not necessarily reflect their true evolutionary status due to significant modification of the parameters by mass transfer between the components.

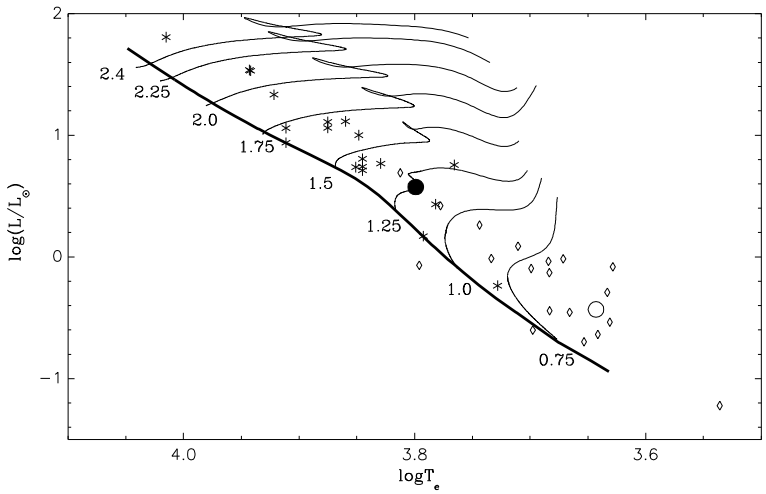

Fig. 9. Positions of the V878 Her components (primary - filled circle, secondary - open) shown among other NCBs of SD1-type from Tian & Chang (2020), with asterisks denoting primaries and diamonds - secondaries. Evolutionary tracks of stars with indicated masses and solar (Z=0.014) metallicity, together with the isochrone of 10^8 years (thick solid line), mimicking ZAMS, are taken from PARSEC models (Bressan et al. 2012).

9. CONCLUSIONS

New radial velocity and light curve data for V878 Her, a near contact partially eclipsing binary, have been simultaneously analysed with the Wilson-

Devinney (WD2003) code. There were two separate LC datasets: One was from the TESS space satellite and the other from a land-based (MAO) observatory. The RV data alone yielded results for K_1 (101.7 ± 4.3 km·s^{-1}), K_2 (219.5 ± 2.4 km·s^{-1}), RV_γ (-34.4 ± 5 km·s^{-1}), and q_{sp} (0.464 ± 0.040). A more rigorous analysis (Wilson 1990) was obtained by simultaneously modeling the TESS light curve data and the RV observations from DAO. This resulted in the best estimates for M_1 ($1.55 \pm 0.18\ M_\odot$), M_2 ($0.69 \pm 0.23\ M_\odot$), R_1 ($1.62 \pm 0.03\ R_\odot$), R_2 ($1.12 \pm 0.02\ R_\odot$), q_{WD} (0.442 ± 0.001), L_1 ($3.75 \pm 0.36\ L_\odot$), and L_2 ($0.37 \pm 0.04\ L_\odot$). Simultaneous analysis with the MAO data yielded similar parameter values but often with greater uncertainties.

Evolutionary calculations indicate that the age of V878 Her is around 1 Gyr. Its progenitor was a detached binary with ZAMS component masses $M_1 \approx 1.66 M_\odot$, $M_2 \approx 0.6 M_\odot$ and initial orbital period $P \approx 1.6$ days. The presently observed mass transfer rate is significantly lower than expected from TRO theory and implies that V878 Her is a first timer which will change into a contact system in the future.

10. ACKNOWLEDGEMENTS

This research has made use of the SIMBAD database operated at Centre de Données astronomiques de Strasbourg, France. This work also presents results from the European Space Agency (ESA) space mission Gaia. Gaia data are being processed by the Gaia Data Processing and Analysis Consortium (DPAC). Funding for the DPAC is provided by national institutions, in particular those participating in the Gaia MultiLateral Agreement (MLA). The Gaia mission website is https://www.cosmos.esa.int/gaia while the Gaia archive website is https://archives.esac.esa.int/gaia. This paper also makes use of data obtained from the Mikulski Archive for Space Telescopes (MAST) at the Space Telescope Science Institute. STScI is operated by the Association of Universities for Research in Astronomy, Inc., under NASA contract NAS5-26555. Support to MAST for these data is provided by the NASA Office of Space Science via grant NAG5-7584 and by other grants and contracts. It is a pleasure to thank the staff members at the DAO (David Bohlender, Dmitry Monen) for their usual splendid help and assistance. The diligence and dedication shown by all associated with these organizations is very much appreciated.

REFERENCES

Alton, K.B., & Stępień, K. 2018, *AcA*, **68**, 449

Agerer, F. & Huebscher, J. 1997, *I.B.V.S.*, **4472**, 1

Agerer, F. & Hübscher, J. 1999, *I.B.V.S.*, **4711**, 1

Agerer, F., Dahm, M. & Hübscher, J. 2001, *I.B.V.S.*, **5017**, 1

Agerer, F. & Hübscher, J. 2002, *I.B.V.S.*, **5296**, 1

Bloomer, R.H. & Ngwele, I.R. 1999 *I.B.V.S.*, **4754**, 1

Bradstreet, D.H. & Steelman, D.P. 2004 *BInary Maker 3, Contact Software (http://www.binarymaker.com).*

Bràt, L. & et al. 2008 *O.E.J.V.S*, **094**, 1
Bressan, A., Marigio, P., Girardi, L., et al. 2012, *Mon. Not. Roy. Astron. Soc.* , **427**, 127
Caldwell, D.A. 2020, *Research Notes of the AAS*, **4**, 201
Diethelm, R. 2010, *I.B.V.S.*, **5945**, 1
Diethelm, R. 2011, *I.B.V.S.*, **5992**, 1
Dvorak, S.W. 2004 *I.B.V.S.*, **5502**, 1
Eggleton, P. P., in *Proc. A.S.P. Conf. Ser.*, No. 90, p.257, eds. Milone, E.F. & Mermilliod, J.-C.
Gaia Collaboration et al. 2021, *Astron. Astrophys.*, **649A**, 1
Ge, H., Hjellming, M.S., Webbink, R.F., Chan, X. & Han, Z., 2010, *Astroph. Journal*, **717**, 72
Hartmann, L.W. & Noyes, R.W. 1987, ARA&A, **25**, 271
Henden, A.A., Welch, D.L., Terrell, D., & Levine, S.E. 2009 *American Astronomical Society Meeting Abstracts*, **41**, 669
Hilditch, R.W., Bell, S.A., Hill, G. & Harries, T.J. 1998, *Mon. Not. Roy. Astron. Soc.*, **296**, 100
Hoffman, D.I., Harrison, T.E., Coughline, J.L. & et al. 2008, *Astron. J.*, **136**, 1067
Hübscher, J., Paschke, A. & Walter, F. 2006, *I.B.V.S.*, **5731**, 1
Hübscher, J. & Walter, F. 2006, *I.B.V.S.*, **5761**, 1
Hübscher, J. & et al. 2010, *I.B.V.S.*, **5918**, 1
Hübscher, J. & Monninger, G. 2011, *I.B.V.S.*, **5959**, 1
Hübscher, J., Lehmann, P.B. & Walter, F. 2012, *I.B.V.S.*, **6010**, 1
Hübscher, J. & Lehmann, P.B. 2015, *I.B.V.S.*, **6149**, 1
Hübscher, J. 2017, *I.B.V.S.*, **6196**, 1
Kaiser, D.H. 1994, *I.B.V.S.*, **4119**, 1
Kaiser, D.H., Lubcke, G. & Williams, D.B. 1996, *I.B.V.S.*, **4284**, 1
Kippenhahn R. & Weigert, A. 1967, *Zs. für Astrophysik*, **65**, 251
Krajci, T. 2005 *I.B.V.S.*, **5592** 1
Kurucz, R.L. 1993, *"New Atmospheres for Modelling Binaries and Disks", in Light Curve Modeling of Eclipsing Binary Stars, E.F. Milone (ed), pp 93-102, Springer, New York*
Kwee, K.K. 1958, *Bulletin of the Astronomical Institutes of the Netherlands*, **14**, 131
Li, K. & et al. 2019, *Res. Astron. Astrophys.*,**19**, 147
Liakos, A., Gazeas, K. & Nanouris, N. 2014, *I.B.V.S.*, **6095**, 1
Lucy, L.B. 1967, *Z. fur Astroph.*, **65**, 89
Lucy, L.B. 1976, *Astroph. Journal*, **205**, 208
Lucy L.B. & Wilson, R.E. 1979, *Astroph. Journal*, **231**, 502
Nagai, K. 2011, *Var. Star Bulletin*, **51**, 5
Nagai, K. 2014, *Var. Star Bulletin*, **56**, 4
Nagai, K. 2021, *Var. Star Bulletin*, **69**, 7
Nelson, R.H. 2005, *I.B.V.S.*, **5602**, 1
Nelson, R.H. 2009, *WDWInT56a: Astronomy Software by Bob Nelson (https://www.variablestarssouth.org/bob-nelson)*
Nelson, R.H. 2010, *"Spectroscopy for Eclipsing Binary Analysis" in The Alt-Az Initiative, Telescope Mirror & Instrument Developments (Collins Foundation Press, Santa Margarita, CA), R.M. Genet, J.M. Johnson and V. Wallen (eds)*
Nelson, R.H. 2013, *Software by Bob Nelson, http://binaries.boulder.swri.edu/binaries/*

Nelson, R.H. 2014, *I.B.V.S.*, **6092**, 1
Nelson, R.H. 2019, *I.B.V.S.*, **6262**, 1
Nelson, R.H. 2020, *New Astron.*, **77**, 101362
Nelson, R.H. 2022, *O.E.J.V.S*, **226**, 1
Nelson, C.A. & Eggleton, P.P. 2001, *Astrophys. Journal*, **552**, 664
Norton, A.J., Wheatley, P.J., West, R.G. & et al. 2007, *Astron. and Astrophys.*, **467**, 785
O'Connell, D.J.K. 1951, *Publ. Riverview Coll. Obs.*, **2**, 85
Pagel, L. 2018a, *I.B.V.S.*, **6244**, 1
Pagel, L. 2018b, *BAV Journal*, **31**, 17
Pagel, L. 2020, *BAV Journal*, **33**, 17
Pagel, L. 2021, *BAV Journal*, **52**, 14
Pagel, L. 2022, *BAV Journal*, **60**, 21
Paschke, A. 2011, *O.E.J.V.S*, **142**, 1
Paschke, A. 2021, *BAV Journal*, **55**, 5
Pecaut, M.J. & Mamajek, E.E. 2013, *Astrophys. J. Supplement*, **208**, 9
Popper, D.M. 1996, *Astrophys. J. Suppl. Ser.*, **106**, 133
Prša & Zwitter 2005, *Astrophys. J.*, **628**, 426
Qian, S. 2001, *Mon. Not. Roy. Astron. Soc.*, **328**, 635
Qian, S. 2003, *Mon. Not. Roy. Astron. Soc.*, **342**, 1260
Ren, J. -J., Raddi, R., Rebassa-Mansergas, A., & et al. 2020, *ApJ*, **905**, 38R
Ricker, G.R., Winn, J.N., Vanderspek, R., Latham, D.W., & et al. 2015, *Journal of Astronomical Telescopes, Instruments, and Systems*, **1**, 014003
Rosner, R., Golub, L., & Vaianna, G.S. 1985, *ARA&A*, **23**, 413
Ruciński, S.M. 1969, *Acta Astron.*, **19**, 245
Ruciński, S.M. 1992, *Astron. J.*, **104**, 1968
Ruciński, S.M. 2004, *"Advantages of the Broadening Function (BF) over the Cross-Correlation Function (CCF)", in Stellar Rotation, Proc. IAU Symp.*, **215**
Samolyk, G. 2017, *J.A.A.V.S.O.*, **45**, 215
Sarna, M.J. & Fedorova, A.V. 1989, *Astr. & Ap.*, **208**, 111
Schlegel, D.J., Finkbeiner, D.P. & Davis, M. 1998, *Astrophys. J.*, **500**, 525
Schlafly, E.F. & Finkbeiner, D.P. 2011, *Astrophys. J.*, **737**, 103
Shaw, J.S. 1990, in C. Ibanoglu ed., Active Close Binaries, Kluwer, p.241
Shaw, J.S. 1994, *Società Astron. Italiana*, **65**, 95
Stefanik, R.P., Latham, D.W., & Torres, G. 1999, *ASPC 185, Precise Stellar Radial Velocities, ed. J.B. Hearnshaw & C.D. Scarfe*, , 354
Stępień, K. 1995, *MNRAS*, **274**, 1019
Stępień, K. 2006, *AcA*, **56**, 199
Stępień, K. 2009, *Mon. Not. Royal Astr. Soc*, **397**, 857
Stępień, K. 2011, *AcA*, **61**, 139
Stępień, K. & Kiraga, M. 2013, *AcA*, **63**, 239
Stępień, K., Pamyatnykh, A.A. & Rozyczka, M. 2017, *Astr. Ap.*, **597**, 87
Tian, X.-M. & Chang, L.-F. 2020, *Pub. Astr. Soc. of Australia*, **37**, e031
van Hamme, W. 1993, *Astron. J.*, **106**, 2096
van Hamme, W., Samec, R.G., Gothard, N.W. et al. 2001, *Astron. J.*, **122**, 3436
Warner, B.D. 2007, *Minor Planet Bulletin*, **34**, 113
Wilson, R.E. 1979, *Astroph. J.*, **234**, 1054
Wilson, R.E. 1990, *Astroph. J.*, **356**, 613
Wilson, R.E. & Devinney, E.J. 1971, *Astroph. J.*, **166**, 605

Yakut, K. & Eggleton, P.P. 2005, *Astroph. J.*, **629**, 1055
Yilmaz, M. & et al. 2009, *I.B.V.S.*, **5887**, 1
Zhu, L.Y., Qian, S.B., Zola, S. & Kreiner, J.M. 2009, *Astron. J.*, **137**, 3574

Kevin B. Alton: Desert Blooms Observatory, 70 Summit Ave., Cedar Knolls, NJ, USA (mail@underoakobservatory.com).